

# Lightweight Learning for Grant-Free Activity Detection in Cell-Free Massive MIMO Networks

ALI ELKESHAWY<sup>1</sup> (*Student Member, IEEE*), HAÏFA FARÈS<sup>1</sup> (*Member, IEEE*), AND AMOR NAFKHA<sup>1</sup> (*Senior Member, IEEE*)

<sup>1</sup>IETR UMR CNRS 6164, CentraleSupélec, Cesson Sévigné 35576, France.

CORRESPONDING AUTHOR: Ali Elkeshawy (e-mail: ali-fekry-ali-hassan.elkeshawy@centralesupelec.fr).

This work was supported from the French National Research Agency (ANR-22-CE25-0015) within the frame of the project POSEIDON.

**ABSTRACT** Grant-free random access (GF-RA) is a promising access technique for massive machine-type communications (mMTC) in future wireless networks, particularly in the context of 5G and beyond (6G) systems. Within the context of GF-RA, this study investigates the efficiency of employing supervised machine learning techniques to tackle the challenges on the device activity detection (AD). GF-RA addresses scalability by employing non-orthogonal pilot sequences, which provides an efficient alternative comparing to conventional grant-based random access (GB-RA) technique that are constrained by the scarcity of orthogonal preamble resources. In this paper, we propose a novel lightweight data-driven algorithmic framework specifically designed for activity detection in GF-RA for mMTC in cell-free massive multiple-input multiple-output (CF-mMIMO) networks. We propose two distinct framework deployment strategies, centralized and decentralized, both tailored to streamline the proposed approach implementation across network infrastructures. Moreover, we introduce optimized post-detection methodologies complemented by a clustering stage to enhance overall detection performances. Our 3GPP-compliant simulations have validated that the proposed algorithm achieves state-of-the-art model-based activity detection accuracy while significantly reducing complexity. Achieving 99% accuracy, it demonstrates real-world viability and effectiveness.

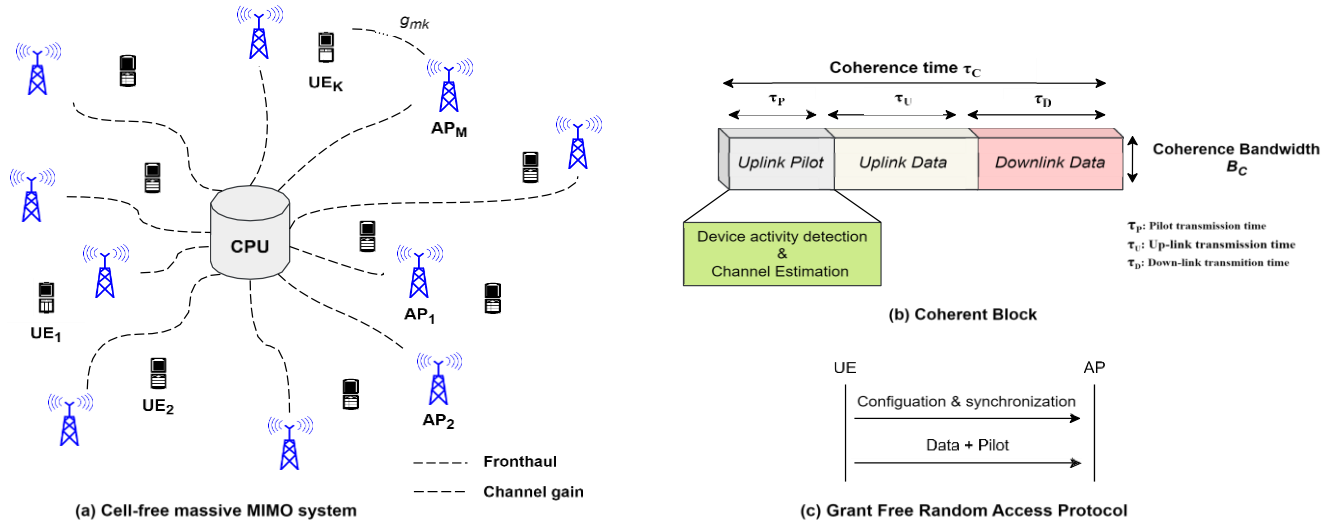
**INDEX TERMS** 6G, Activity Detection, Grant-Free Random Access, Cell-Free massive MIMO Networks, Deep Learning, massive Machine-Type Communications, Sparsity, Pareto Front.

## I. INTRODUCTION

**A**N important step toward adopting internet of things (IoT) applications has been taken with the introduction of mMTC services [1]. This marks the beginning of a new era where devices, constrained by limited memory and energy availability, send small amounts of data sporadically or regularly at short intervals. The widespread proliferation of these devices in large areas presents significant challenges for current wireless networks, especially when it comes to managing the connectivity of such a vast number of connected devices. Within this context, mMIMO technology provides a promising solution to overcome mMTC challenges by significantly improving network coverage and supporting higher device densities, making it a key enabler for future wireless communication systems [2], [3].

GB-RA techniques have been extensively investigated [4]–[6], and it is well established that each device must select a preamble from a limited set of orthogonal sequences to join the wireless network. However, since the number of orthogonal sequences is finite, caused by restricted coherence time and sequence length, there is an increased probability that two or more devices will choose the same sequence, resulting in collision and consequently, wireless access failure [7].

Thus, many grant-free (GF) access strategies have been proposed to solve the limitations of GB-RA techniques [8]. These strategies allow devices to join a wireless network without express permission. In GF scenarios, every device is assigned a unique non-orthogonal pilot sequence, avoiding the constraint of orthogonal sequence assignment because of the short channel coherence time. Therefore, GB-RA is seen


**FIGURE 1.** Cell-free network model for mMTC.

as a feasible method to guarantee network connectivity by effectively controlling non-orthogonal pilot interference and reducing network access latency [9]. Accurate channel estimation is crucial for efficient data communication in mMTC networks, which requires the detection of active devices, a task heavily affected by the sparse activity patterns typical of machine-type devices. We are investigating techniques for identifying which devices are actively transmitting in a given time slot within a GF access system. Our focus is on sparse support recovery methods, which allow us to efficiently detect the small number of active devices among a larger pool of potential transmitters.

Techniques for identifying sparse support can be categorized into three primary groups: compressive sensing (CS) methods [10]–[17], covariance-based (CV) approaches [18]–[21], and data-driven strategies [22], [23]. These methodologies represent distinct paradigms for addressing the challenge of sparse support recovery in various applications. Detecting active devices within grant-free random access for mMTC in CF-mMIMO networks, as shown in Fig. 1 (c), presents considerable difficulties, underscoring the necessity for sophisticated detection methods. GF access is a communication protocol that allows devices to transmit without prior scheduling permissions from the network controller, advantageous for environments requiring low latency and minimal signaling overhead, such as mMTC applications. In CF-mMIMO systems, as illustrated in Fig. 1(a), the stability provided by coherent blocks is critical to efficiently decode unscheduled transmissions from multiple devices enabled by GF access, thereby enhancing network performance and scalability.

### A. RELATED WORKS

In this section, a concise overview of the literature on sparse support recovery relevant to GF-RA protocols is provided. The AD problem is formulated as a compressive sensing

problem in [10], [11], with the goal of reconstructing a sparse signal from a restricted number of measurements. In GF-RA, these measurements correspond to the signal received at a given AP, while the sparse signal represents the sporadic activity patterns of the MTC devices.

Several algorithms based on CS have been developed for joint channel estimation and device activity detection; among them, we can mention greedy pursuit algorithms which are widely used for sparse signal recovery [12], [13] and the approximate message passing (AMP) algorithm [14]. Additionally, the sparse inference problem in the compressive sensing context can be formulated as a least absolute shrinkage and selection operator (LASSO) optimization problem [24], which can be addressed using various algorithms, including convex relaxation methods such as the iterative soft thresholding algorithm (ISTA) and its accelerated version, FISTA (fast iterative shrinkage-thresholding algorithm) [25]. In [15], authors proposed a CS-based method to efficiently handle the massive number of devices in non-coherent mMIMO systems, that simultaneously transmit data without requiring dedicated resources or scheduling grants from the base station.

The CV-based method is presented in [18], showing better performance than current CS-based techniques. In fact, while CS techniques are well-suited for scenarios with moderate device activity and sufficient pilot resources, the covariance-based approach provides a more scalable and flexible solution for GF-RA in ultra-dense mMTC networks, particularly when the number of active devices exceeds the pilot sequence length. Moreover, in [19], authors suggest a CV-based method for joint activity and data detection, along with a performance analysis that underscores its superior advantages compared to other existing methods.

In [20], authors make several important contributions to the field of improving activity detection for mMTC in CF-mMIMO networks. They investigated GF-RA and modeled

TABLE 1. List of acronyms.

3GPP	3rd generation partnership project
6G	Sixth-Generation
AD	Activity Detection
AMP	Approximate Message Passing
ANN	Artificial Neural Networks
APs	Access Points
CF-mMIMO	Cell-Free Massive Multiple-Input Multiple-Output
CS	Compressive Sensing
CS-MUD	CS Multi-User Detection
CDF	Cumulative Distribution Function
CPU	Central Processing Unit
CV	Covariance-Based
DL	Deep Learning
DNN	Deep Neural Network
FA	False Alarm
FISTA	Fast Iterative Shrinkage-Thresholding Algorithm
GB-RA	Grant-based Random Access
GF	Grant-Free
GF-RA	Grant-Free Random Access
GPU	Graphics Processing Unit
IoT	Internet of Things
ISTA	Iterative Soft Thresholding Algorithm
LASSO	Least Absolute Shrinkage and Selection Operator
LSF	Large-Scale Fading
MAC	Multiply-Accumulate
MIMO	Multiple-Input Multiple-Output
MD	Miss Detection
MMV	Multiple Measurement Vector
mMTC	Massive Machine-Type Communication
ML	Machine Learning
NN	Neural Network
ReLU	Rectified Linear Unit
ROC	Receiver Operating Characteristics
SLP	Single-Layer Perceptron
SSF	Small-Scale Fading
UMa-LOS	Urban Macro Line-Of-Sight
ZC	Zadoff-Chu

device activity detection as a maximum likelihood detection problem. Their approach, initially introduced in [21], focuses on device AD via a single dominating AP, marking a noteworthy advancement. In addition, authors propose a novel clustering-based activity detection technique that promises to enhance detection efficiency at the expense of higher computation complexity on the central processing unit (CPU). Their results highlight how CF-mMIMO networks can greatly improve activity identification when a large number of devices are connected, demonstrating the potential of this method in future wireless networks aiming to facilitate IoT services.

To greatly improve device activity detection in mMTC scenarios under GF-RA protocols, authors in [22] suggest a

dual-strategy method. Their work aims at robust and efficient AD by introducing two deep learning (DL) algorithms for sparse support recovery. They include a feature selection step, which focuses on selecting various pilot sequences with good cross-correlation properties to optimize the neural network (NN) design. Their results show how effective Zadoff-chu (ZC) sequences are as pilots, exhibiting higher activity detection accuracy with less computing load and providing a viable way to handle massive connectivity issues.

To overcome the computational complexity of CS multi-user detection (CS-MUD) in huge mMTC systems, in [23], authors present an innovative deep learning technique utilizing a specially designed block-restricted activation nonlinear unit, suitable to efficiently leverage the block sparse structure inherent in systems with many antennas or wide bandwidths. This approach enhances the performance of CS-MUD by offering a ten-fold reduction in computing time.

### B. PAPER CONTRIBUTIONS

Motivated by the above discussion, in this paper, we propose a learning-based model to improve activity detection in grant-free random access for mMTC in CF-mMIMO network. Our main contributions can be resumed as follows:

- A robust learning-based model is proposed to allow accurate AD of the device in a GF-RA. This model leverages a single-layer perceptron (SLP) architecture to efficiently process symbols received during the random access slot, focusing on sparse support recovery for activity detection.
- Two deployment strategies have been developed for the proposed model: decentralized and centralized. In the decentralized approach, the model is distributed across all access points (APs) in the network, enabling localized and independent processing at each node. In contrast, the centralized approach consolidates data from all APs into the CPU, where computations are performed in a unified manner. While the two strategies differ in their operational workflows, they are built upon the same model architecture, ensuring consistency in performance and functionality.
- The architectural parameters of the proposed model are carefully analyzed through numerical evaluation to ensure optimal performance. This process aims to achieve high accuracy in activity detection while mitigating the risk of overfitting, ensuring the model's reliability and generalization across diverse scenarios.
- Recognizing the computational complexities associated with involving all APs in device activity detection within a CF-mMIMO network, we propose a clustering method to improve efficiency and performance. The method is rigorously developed and evaluated under both decentralized and centralized strategies, addressing various implementation considerations. By carefully selecting a subset of APs with strong channel conditions for each device rather than engaging the entire network,

the clustering approach optimizes the detection process. Additionally, this method is designed to operate independently of the core algorithm, effectively decoupling the clustering process and enhancing scalability.

- An extended analysis is conducted to evaluate the performance of various activity detection algorithms, including the proposed learning-based model and CV-based methods from the literature [25], within both CF-mMIMO and co-located mMIMO. These algorithms are rigorously tested under realistic scenarios, such as dense AP deployments, varying cell area sizes, and power-limited mMTC conditions. The results show that the proposed approach delivers improved performance compared to the methods outlined in [20], demonstrating its effectiveness in challenging network environments.

The remainder of this paper is structured as follows: Section II introduces the system model. Section III provides a detailed description of the DL framework, including the proposed lightweight deep neural network (DNN) model architecture and its deployment in centralized or distributed manner. Section IV presents the numerical results and demonstrating the effectiveness of the proposed algorithms. Finally, the paper is concluded in Section V.

## II. SYSTEM MODEL

Consider a CF-mMIMO wireless network consisting of  $M$  APs, each equipped with  $N$  antennas, distributed across the coverage area and connected via front-haul connections to CPU. The APs serve a set of  $K$  single-antenna MTC devices. Due to the sporadic nature of traffic in the mMTC massive access scenario, only a small fraction of the  $K$  devices will be active at a given time instant.

In the present work, we assume that each device transmits independently with an activation probability,  $\epsilon \ll 1$ . The activity status of the  $k$ -th device is denoted by  $a_k \in \{0, 1\}$ , where  $k \in \{1, 2, \dots, K\}$  and  $a_k = 1$  indicates that the  $k$ -th device is active, and  $a_k = 0$  indicates that the  $k$ -th device is not active in the timeslot. The activation and inactivation probabilities of the  $k$ -th device are denoted by  $\Pr(a_k = 1) = \epsilon$ , and  $\Pr(a_k = 0) = (1 - \epsilon)$  respectively. The resulting vector  $\mathbf{a} = (a_1, a_2, \dots, a_K)^t$  represents the activity of the  $K$  devices, and it is sparse vector due to the sporadic communication nature of mMTC. The set of active devices is represented by  $\mathbf{A}$ , where  $\mathbf{A} = \{k \in \{1, 2, \dots, K : a_k = 1\}$ . Additionally, it is noteworthy that the activity follows the Bernoulli distribution.

Considering the geographic distribution of the devices, we assume independent channel realizations between devices and access points. Moreover, we suppose that the  $N$  antennas at each AP are sufficiently separated, so that each path provides an independent fading. The channel gain between  $k$ -th device and  $n$ -th antenna of the  $m$ -th access point is

denoted by  $g_{mk}^{(n)}$  and it can be modeled as follows:

$$g_{mk}^{(n)} = \beta_{mk}^{1/2} \times h_{mk}^{(n)} \quad (1)$$

where  $\beta_{mk}$  is defined as the large-scale fading (LSF) coefficient between the  $m$ -th access point and the  $k$ -th device as specified in 3GPP standard [26], and it is expressed as :

$$\begin{aligned} \beta_{mk} &= PL + F_{mk} \\ PL &= \begin{cases} PL_1, & 10m \leq d_{2D} \leq d'_{BP} \\ PL_2, & d'_{BP} < d_{2D} \leq 5km \end{cases} \\ PL_1 &= 28.0 + 22 \log_{10}(d_{3D}) + 20 \log_{10}(f_c) \\ PL_2 &= 28.0 + 40 \log_{10}(d_{3D}) + 20 \log_{10}(f_c) \\ &\quad - 9 \log_{10} (d'_{BP})^2 + (h_{BS} - h_{UT})^2, \end{aligned} \quad (2)$$

The LSF coefficient  $\beta_{mk}$  consists of two elements: the standard path loss model  $PL$ , pertinent to urban macro line-of-sight (UMa-LOS) conditions, and the shadow fading component modeled as a gaussian random variable as  $F_{mk} \sim \mathcal{N}(0, \sigma_{sh}^2)$ . The path loss model is contingent on the horizontal distance  $d_{2D}$ , gauging the separation between each device  $k$  and access point  $AP_m$ , with  $d'_{BP}$  denoting the breakpoint distance beyond which the model switches from model  $PL_1$  to model  $PL_2$ , accounting for the height differences between devices and access points. Furthermore, the small-scale fading (SSF) coefficient is denoted by  $h_{mk}^{(n)} \sim \mathcal{CN}(0, 1)$  and remains constant for some consecutive activity vectors, where the activity can change up to multiple times before the channel changes. We assume that the LSF coefficient parameters  $\beta_{mk}$  are known at the CPU, as considered in [20]. The assumption builds upon the methods proposed in [27], [28], which provide key algorithms for estimating the LSF coefficients. In the sequel of this paper, we consider a block fading scenario where each channel coefficient remains unchanged during a coherence time interval, and each channel realization is independent of all other realizations.

In the uplink of a narrow-band mMTC system within a square area of  $D \times D$  km<sup>2</sup>, assigning orthogonal pilot sequences to devices is unfeasible due to limited channel coherence time  $\tau_c$  defined as the duration over which the channel remains approximately constant. The mMTC network typically supports a large number of devices, far exceeding the number of symbols  $T_c$  that can be transmitted in the coherence block, as illustrated in Fig. 1(b), where  $T_c$  is defined as  $T_c = \tau_c \times B_c$ , with  $B_c$  representing the coherence bandwidth. The phenomenon of pilot contamination arises because each active device transmits non-orthogonal pilot sequences  $\mathbf{s}_k$  during a random access slot. The sequences are drawn from a gaussian distribution, i.e.,  $\mathbf{s}_k \in \mathbb{C}^{L \times 1}$ , where  $L$  is the pilot sequence length. The length  $L$  constitutes a specific reserved portion, such as  $\Delta$  %, of the coherence block. All frames are assumed to be received synchronously at the access points.



The received signal  $\mathbf{y}_{mn} \in \mathbb{C}^{L \times 1}$  at the  $n$ -th antenna of the  $m$ -th access point can be expressed as :

$$\begin{aligned} \mathbf{y}_{mn} &= \sum_{k=1}^K a_k \rho_k^{1/2} \mathbf{g}_{mn}^{(n)} s_k + \mathbf{w}_{mn} \\ &= \mathbf{S} \mathbf{D}_a \mathbf{D}_\rho^{1/2} \mathbf{g}_{mn} + \mathbf{w}_{mn}, \end{aligned} \quad (3)$$

where  $\mathbf{S} = [\mathbf{s}_1 \mathbf{s}_2 \dots \mathbf{s}_K] \in \mathbb{C}^{L \times K}$  represents the collection of all pilot sequences. The power transmitted by device  $k$  is denoted as  $\rho_k$ , and the matrix  $\mathbf{D}_\rho = \text{diag}(\rho_1, \rho_2, \dots, \rho_K)$  is the diagonal matrix containing these powers. The matrix  $\mathbf{D}_a = \text{diag}(\mathbf{a})$  represents the activity matrix. The channel vector  $\mathbf{g}_{mn} = [g_{m1}^{(n)}, g_{m2}^{(n)}, \dots, g_{mK}^{(n)}]^t \in \mathbb{C}^{K \times 1}$  describes the channel between all  $K$  MTC devices and the  $n$ -th antenna of the  $m$ -th AP, where  $[\cdot]^t$  indicates the transpose operation. Lastly,  $\mathbf{w}_{mn} \sim \text{CN}(0, \sigma^2 \mathbf{1}_L)$  is an  $L$ -dimensional complex gaussian random vector, representing noise at  $n$ -th antenna of the  $m$ -th AP. Thus, the signal  $\mathbf{Y}_m \in \mathbb{C}^{L \times N}$  received at the  $m$ -th access point can be expressed as:

$$\mathbf{Y}_m = \mathbf{S} \mathbf{D}_a \mathbf{D}_\rho^{1/2} \mathbf{G}_m + \mathbf{W}_m, \quad (4)$$

where  $\mathbf{G}_m = [\mathbf{g}_{m1}, \mathbf{g}_{m2}, \dots, \mathbf{g}_{mN}] \in \mathbb{C}^{K \times N}$  is the channel matrix between all devices and the  $m$ -th AP, and  $\mathbf{W}_m = [\mathbf{w}_{m1}, \mathbf{w}_{m2}, \dots, \mathbf{w}_{mN}] \in \mathbb{C}^{L \times N}$  is an additive Gaussian noise matrix. Then, by omitting the index  $m$ , the received signal at any access point can be expressed as:

$$\mathbf{Y} = \mathbf{S} \mathbf{X} + \mathbf{W}, \quad (5)$$

where  $\mathbf{X} = \mathbf{D}_a \mathbf{D}_\rho^{1/2} \mathbf{G}_m \in \mathbb{C}^{K \times N}$  is a row sparse matrix. The device activity detection problem aims to find the most likely activity vector given the code book of pilot sequences  $\mathbf{S}$ . This process involves identifying the indices of the nonzero entries (i.e., rows) in the sparse matrix  $\mathbf{X}$ . These indices represent the support of  $\mathbf{X}$ , i.e., the locations of the non-zero rows. The support of matrix  $\mathbf{X}$  can be defined as follows:

$$\text{supp}(\mathbf{X}) = \left. \left. k \in \mathbf{N}^+ \mid \mathbf{x}_{k, \cdot} \neq \mathbf{0} \right\} \right\}, \quad (6)$$

where  $\mathbf{x}_{k, \cdot}$  denotes the  $k$ -th row of the sparse matrix  $\mathbf{X}$ . we can denote that each column of row sparse matrix  $\mathbf{X}$  shares the same locations of non-zero entries. Therefore, finding the support of  $\mathbf{X}$  from the array received matrix  $\mathbf{Y}$ , comprising all received vectors, and the matrix  $\mathbf{S}$  which is considered as the sensing matrix, can be seen as a sparse support recovery problem of the multiple measurement vector (MMV) model corrupted by additive noise. Consequently, the MMV problem can be formulated as follows [29]:

$$P_0 : \min_{\mathbf{X}} \|\mathbf{X}\|_0 \quad \text{s.t.} \quad \mathbf{Y} = \mathbf{S} \mathbf{X}, \quad (7)$$

where,  $\|\mathbf{X}\|_0 = |\text{supp}(\mathbf{X})|$ . The  $P_0$ -minimization problem is NP-hard due to the non-convexity of the L0-pseudo-norm. Common approximations, such as convex relaxation methods and iterative algorithms, as well as various other approaches, offer varying degrees of computational efficiency to tackle the  $P_0$  computation complexity. The minimization problem

$P_0$  can be addressed using DL, a specialized branch of machine learning (ML), particularly for detecting sporadic device activity in mMTC systems.

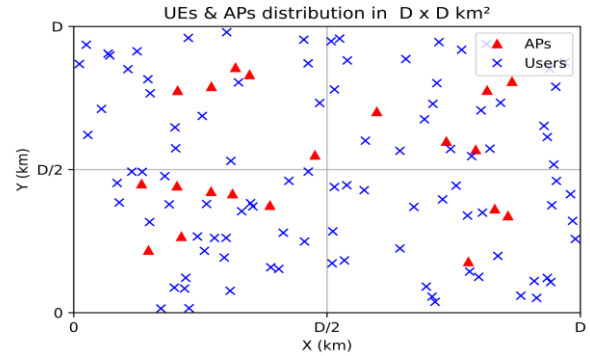


FIGURE 2. Distribution of devices and access points within the network.

### III. DEEP LEARNING FRAMEWORK

A lightweight DL framework based on input I-Q received samples is proposed to address AD challenges in mMTC systems, with a particular focus on sparse recovery tasks. This framework typically employs NN architectures capable of capturing complex input-output relationships, with the possibility of utilizing multiple layers to enhance detection accuracy and efficiency. However, a specific architecture will be determined based on further analysis and experimentation. Particularly, regression analysis using a DL architecture involves mapping an input signal to a specific output. A more capacity-efficient approach arises from recognizing that a sparse vector can be efficiently derived using the least squares estimator, notably when its support is known. Instead of directly predicting the activity vector  $\mathbf{a}$ , we propose using a DL model to approximate the mapping between  $\mathbf{Y}$  and the support of row sparse matrix  $\mathbf{X}$ , which is the support of sparse activity vector  $\mathbf{a}$ . This intentional reformulation transforms the problem into a multi-binary label classification task, which is particularly effective for identifying active devices.

In the following subsections, we provide an overview of the data generation process, the adopted lightweight DNN architecture with diverse input features designed for efficient AD, the APs clustering process, along with an explanation of framework deployment strategies I and II. We ended this section by detailing the training phase.

#### A. DATA GENERATION

The challenge of gathering large amounts of real data is a major problem when using DL in wireless communication systems. Fortunately, synthetic data can train DNN to tackle the  $P_0$  minimization problem presented in (7). In this study, we prioritized accurately replicating real-world conditions during data generation phase. Initially, this required assigning MTC devices to a specified square area of  $D \times D$

**TABLE 2.** Comparison of centralized and decentralized activity detection strategies

	Activity Detection Framework	
	Strategy I	Strategy II
<b>Detection framework</b>	Decentralized	Centralized
<b>Model deployment type</b>	AP-centric	CPU-centric
<b>Signal selection</b>	Disabled	Enabled
<b>Input signal representation</b>	$Y_m$	$Y_i/i \in S_u \subset \{1, 2, \dots, M\},  S_u  = T$
<b>Signal exchange scheme</b>	Prediction only	All AP-signals
<b>Clustering approach</b>	Post-model prediction	Pre-model prediction
<b>Post-processing method</b>	Processing I	Hard decision mechanism
	Processing II	

km<sup>2</sup>, with APs placed to maintain realistic AP-AP and MTC device-AP distances, ensuring appropriate spacing, edge distance, and coverage distribution, as depicted in Fig. 2.

As the geographic topology was set up, the LSF effects were calculated using the 3GPP standard UMA criteria, incorporating the LOS condition. This was important because it highlighted how complex signal transmission is in metropolitan environments, where massive structures (distance attenuation, shadowing) have a significant impact on received signal behavior. Furthermore, the probability of each device being active was indicated by their activity status, calculated using a binomial distribution. As in [20], this study ensures that 95% of active devices gain access to the network by guaranteeing that all active devices achieve a target signal-to-noise ratio (SNR) at their dominant access point. The dominant AP can be defined as the access point that provides the strongest channel gain.

To model the SSF, two approaches are available to generate rayleigh fading channels. The first approach allows fading to vary based on device activity, ensuring an accurate depiction of real conditions and evaluating the system's reaction to fluctuations. The second approach adopts a stable fading model for multiple device activities. Using previous approaches facilitates an in-depth evaluation of system performance under both dynamic and stable scenarios, yielding valuable insights into its overall performance.

Finally, the signal received at each AP was calculated using (4), which combined the transmitted pilot sequences, the large and small scale fading effects, and the additive Gaussian noise. Through this extensive data generation process, we developed a reliable dataset, which was key to evaluating the proposed algorithm's performance in realistic CF-mMIMO network simulations.

## B. DEEP NEURAL NETWORK

A DNN is a widely used form of DL that consists of artificial neural networks (ANN) with multiple layers between the input and output layers. The lightweight DNN architecture, shown in Fig. 3, includes an input layer that processes incoming data. This input data is defined as the signal representation, which can vary depending on the specific activity detection strategy being implemented. Table 2 provides a detailed outline of the different input signal representations used for both centralized and decentralized strategies within the AD framework.

The proposed architecture comprises  $Z$  densely connected hidden layers, each containing  $V$  nodes. These hidden layers are followed by a concatenation layer, which groups and resizes their outputs based on the input signal representation (as detailed in Table 2). The input to the architecture can be either a single signal  $\mathbf{Y}$  or multiple signals  $\mathbf{Y}_i$ , where  $i \in S_u \subset \{1, 2, \dots, M\}$  and  $|S_u| = T$ . Here,  $T$  represents the cluster size, which will be explained later. Each input type corresponds to a hidden layer output, which then feeds into the concatenation layer. Finally, the architecture includes an output layer consisting of  $K$  neurons, responsible for predicting the activity descriptor vector.

Based on (20), the hidden layers in the model employ the rectified linear unit (ReLU) as their activation function because it is widely used due to its ability to introduce non-linearity while being computationally efficient, as it supports the use of back propagation for efficient learning in complex and deep network architectures.

$$\text{ReLU}(c) = \max(0, c). \quad (8)$$

In addition, the sigmoid activation function is employed in the output layer because it plays a crucial role in binary classification tasks. This decision is based on the particular ability to perform binary classification for each device in

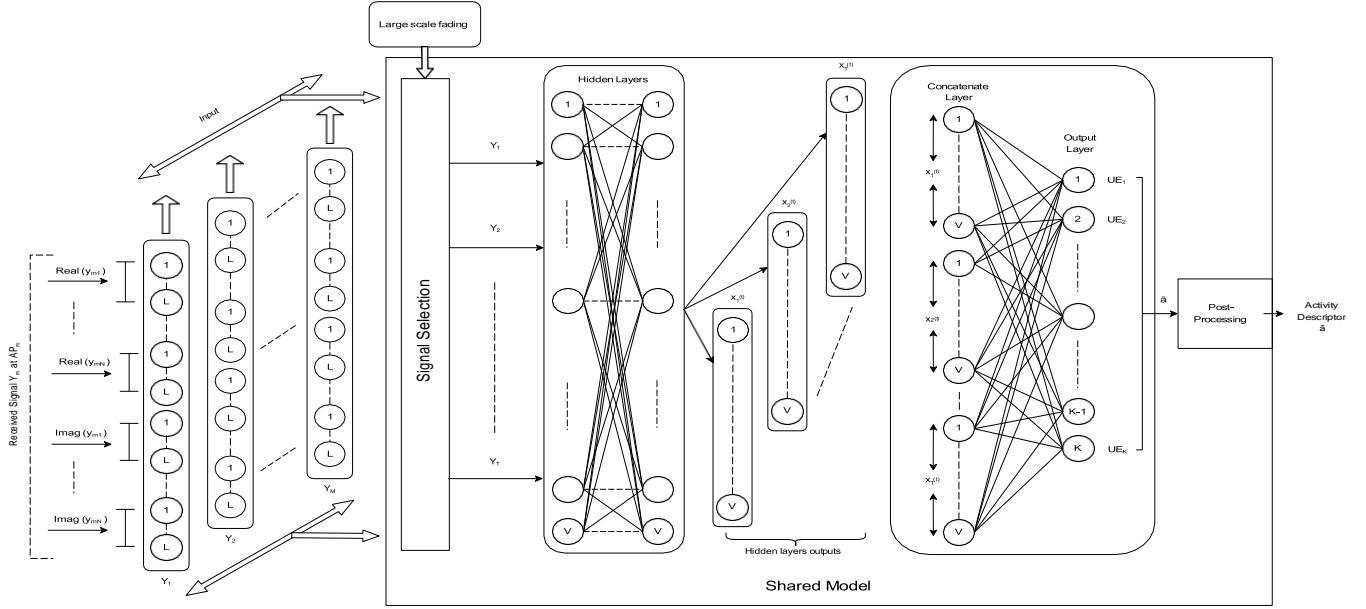


FIGURE 3. Architecture of the DNN algorithm proposed for device activity detection.

order to identify their activities, and it is provided by:

$$\text{Sigmoid}(c) = \frac{1}{1 + e^{-c}}. \quad (9)$$

The input and output dimensions of the DNN are primarily determined by several key criteria. The input depends on  $L$ ,  $N$ , and  $T$ . On the other hand, the output is determined solely by  $K$ . Consequently, any changes in these parameters require retraining for the network to effectively adapt.

The weight matrices and bias vectors, which are the parameters of the DNN layers, are now introduced. We define the weight matrices according to the dimensions of the inputs and outputs of each layer as follows:

The weight matrix connecting the input layer to the first hidden layer is  $\mathbf{U}_1 \in \mathbb{R}^{V \times 2NL}$ , with the input determined by the strategy outlined in Table 2. Whether the input consists of a single signal or multiple signals from the cluster  $\mathbf{Y}_i$ , the same weight matrix is used. This ensures that the number of parameters remains constant, unaffected by the number of signals  $T$  fed into the model.

For subsequent hidden layers, denoted as  $1, 2, \dots, Z$ , the weight matrices are defined as  $\mathbf{U}_2 \in \mathbb{R}^{V \times V}$ ,  $\mathbf{U}_3 \in \mathbb{R}^{V \times V}$ , ...,  $\mathbf{U}_Z \in \mathbb{R}^{V \times V}$ , where  $Z$  represents the total number of hidden layers. Following the hidden layers, a concatenation layer is introduced as a virtual layer that rearranges the outputs without adding any weights or trainable parameters. The output layer, denoted as  $(Z + 1)$ , has a weight matrix  $\mathbf{U}_{Z+1} \in \mathbb{R}^{K \times TV}$ , where  $T$  is the cluster size, and  $V$  is the number of nodes per hidden layer. In the same way, the bias-valued vectors are  $\mathbf{b}_1 \in \mathbb{R}^{V \times 1}$ ,  $\mathbf{b}_2 \in \mathbb{R}^{V \times 1}$ , ...,  $\mathbf{b}_Z \in \mathbb{R}^{V \times 1}$  and  $\mathbf{b}_{Z+1} \in \mathbb{R}^{K \times 1}$ . Considering this, we use the DNN parameters to define the set by:

$$\vartheta = \{\mathbf{U}_z, \mathbf{b}_z\}, \quad z = 1, 2, 3, \dots, Z \quad (10)$$

Finding the number of trainable parameters in the DNN method is feasible when one knows  $\vartheta$ . The number of trainable parameters is determined by taking into account the values of the bias vectors and the weights matrices:

$$\vartheta(K, L, N, V, Z, T) = (Z - 1)V^2 + (2NL + TK + Z)V + K. \quad (11)$$

To process the outputs  $\tilde{\mathbf{a}}$  of the DNN, which are probability values within the range  $[0, 1]$ , a post-processing block is introduced at the output of the algorithm. This block calculates the estimate of the activity descriptor in its original domain, denoted as  $\hat{\mathbf{a}}$ , as defined in Fig. 3.

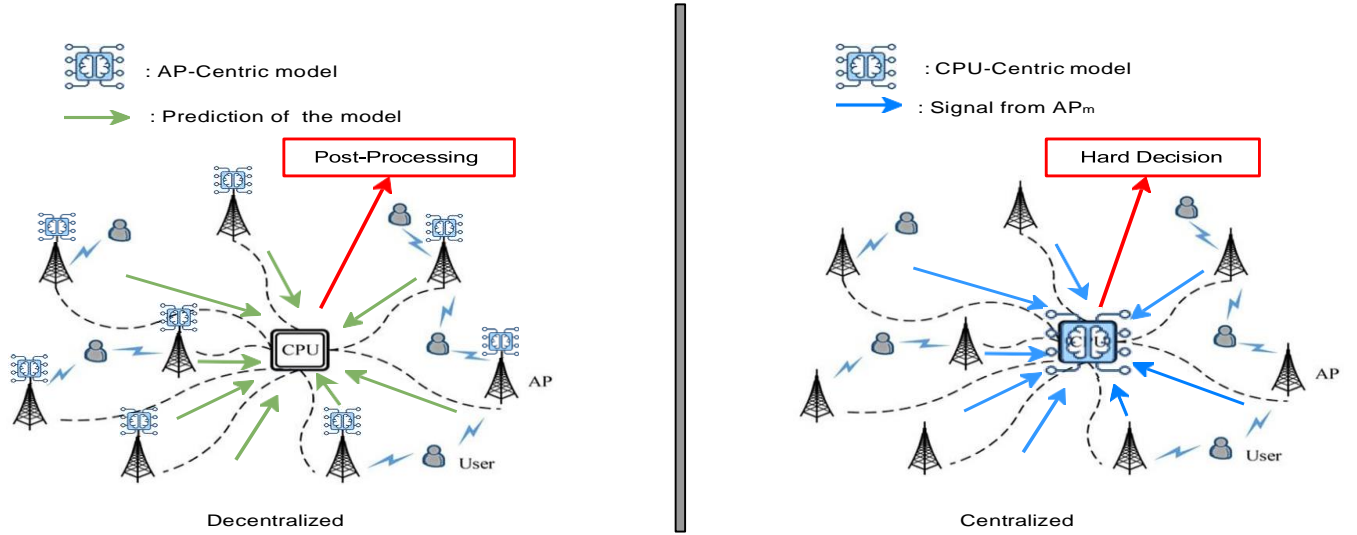
In the process of detecting device activity, two primary types of errors can occur. The first is a false alarm (FA), which happens when a device that is not active is incorrectly identified as active. The second type is a miss detection (MD), occurring when an active device is wrongly classified as inactive. The likelihoods of both FA and MD are determined using a specific hard decision threshold  $\tau$ .

$$P_{\text{FA}}(\tau) = \Pr(\hat{a}_k = 1 | a_k = 0) \quad (12)$$

$$P_{\text{MD}}(\tau) = \Pr(\hat{a}_k = 0 | a_k = 1) \quad (13)$$

The probability of error within each random access slot is affected by the varying number of active devices, which in turn alters the frequency of specific error types. This variability is encapsulated in the error probability function that is expressed using the false alarm and miss detection probabilities related to the threshold  $\tau$  and the probability of activation  $\varepsilon$  as:

$$P_E(\tau, \varepsilon) = (1 - \varepsilon)P_{\text{FA}}(\tau) + \varepsilon P_{\text{MD}}(\tau) \quad (14)$$


**FIGURE 4.** Signal exchange scheme.

### C. CLUSTERING-BASED ACTIVITY DETECTION

Traditional activity detection algorithms rely on data from a single AP per device. In CF-mMIMO networks, utilizing all APs for activity detection is more effective but computationally expensive.

A clustering-based approach for GF-RA, as proposed in [20], groups APs with strong channels to each device, requiring accurate estimates of the LSF coefficients  $\beta_{mk}$ . These coefficients are used to determine the best cluster for each device and within the model to predict activity by solving a polynomial equation of degree  $2T - 1$ , where  $T$  is the number of APs per device cluster. While efficient, this method becomes computationally intensive as the number of devices and cluster sizes increase.

The methodology presented refines the previously stated approach by maintaining the optimal cluster selection per device while decoupling the clustering framework from the DNN model learning phase. The dynamic cluster selection is performed by the CPU in both strategies, independently of the model, to enhance detection accuracy. Specifically, clustering is applied post-prediction in the first strategy and pre-prediction in the second. This separation improves flexibility and efficiency in activity detection for CF networks, significantly reducing computational complexity.

### D. STRATEGY I: DECENTRALIZED

In this approach, the steps of the model are outlined in Table 2 and illustrated on the left side of Fig. 4. The framework operates as follows:

- The model functions in a distributed manner, with a copy deployed on each of the  $M$  APs in the network.
- The architecture in Fig. 3 is simplified by disabling the signal selection block. Each AP  $m$  directly uses the signal it receives as input.

- At AP  $m$ , the model processes the received signal  $\mathbf{Y}_m = [\mathbf{y}_{m1}, \mathbf{y}_{m2}, \dots, \mathbf{y}_{mN}] \in \mathbf{C}^{L \times N}$ , consisting of the real and imaginary components of signals at each antenna  $n$ . This input is passed through the hidden layers, producing a single extracted feature. Since there are no multiple inputs, the concatenation layer has no effect, and the output layer predicts the activity descriptor vector  $\tilde{\mathbf{a}}$  for all devices.
- This process is independently performed by all APs, resulting in  $M$  activity descriptor vectors.
- No clustering is applied at this stage. As shown in Fig. 4, the  $M$  predicted vectors are exchanged with the CPU. At the CPU, each device  $k$  will have  $M$  predicted activity values, represented as  $\tilde{\mathbf{a}}_{\mathbf{M}\mathbf{k}} = (\tilde{a}_{1k}, \tilde{a}_{2k}, \dots, \tilde{a}_{Mk})$ .
- A post-prediction clustering process is then applied. For each device  $k$ , the CPU selects the  $T$  best predicted values  $\tilde{\mathbf{a}}_{T\mathbf{k}} = (\tilde{a}_{1k}, \tilde{a}_{2k}, \dots, \tilde{a}_{Tk})$  out of  $M$ , based on the large-scale fading coefficients  $\beta_{mk}$  known at the CPU. These predicted values fall within the range  $[0, 1]$ .
- Using the  $T$  selected predicted values, a post-processing method determines the final estimated activity of device  $k$ , denoted as  $\hat{a}_k$ .

Two different methods are employed in this approach for post-processing:

**Processing I:** This method consists of two blocks a hard decision phase followed by a fusion rule function.

- The hard decision mechanism applies a threshold  $\tau \geq 0$  to binarize the  $T$  predicted values for device  $k$ :

$$\bar{a}_{tk} = \begin{cases} 0, & \text{if } \tilde{a}_{tk} < \tau, \\ 1, & \text{if } \tilde{a}_{tk} \geq \tau. \end{cases} \quad (15)$$

The binary outputs are represented as  $\bar{\mathbf{a}}_{T\mathbf{k}} = (\bar{a}_{1k}, \bar{a}_{2k}, \dots, \bar{a}_{Tk})$ .



- The binary outputs are then processed by a fusion rule function, which can be AND, OR, or Majority. Majority rule is chosen for its balanced performance, where a device is considered active if the majority ( $T/2$ ) of APs in the cluster detect activity. The output of the fusion rule provides the final estimated activity  $\hat{a}_k$  of device  $k$ .

**Processing II:** This method consists of two blocks a ponderation function block followed by a hard decision phase.

- The goal of the ponderation function is to calculate a final prediction  $\hat{a}_k$  for device  $k$ , which combines multiple predictions made by a cluster of  $T$  APs. These predictions are weighted based on the quality of the channel between the device and each AP. The final prediction is given by:

$$\hat{a}_k = \sum_{t=1}^T w_{tk} \tilde{a}_{tk}, \quad (16)$$

where  $w_{tk}$  represents the weight assigned to the  $t$ -th AP for device  $k$ .

- The weight  $w_{tk}$  reflects the LSF quality (signal strength or reliability) between the  $t$ -th AP and device  $k$ . To ensure the contributions of all APs in the cluster sum to 1, the weight is normalized as follows:

$$w_{tk} = \frac{\beta_{\text{best},tk}}{\sum_{t=1}^T \beta_{\text{best},tk}}. \quad (17)$$

- The hard decision mechanism applies a threshold  $\tau \geq 0$  to binarize the weighted outputs for each device  $k$ , denoted as  $\hat{a}_k$  to provide the final estimated activity  $\hat{a}_k$  of device  $k$ :

$$\hat{a}_k = \begin{cases} 0, & \text{if } \hat{a}_k < \tau, \\ 1, & \text{if } \hat{a}_k \geq \tau. \end{cases} \quad (18)$$

### E. STRATEGY II: CENTRALIZED

In this approach, the steps of the model are outlined in Table 2 and shown on the right side of Fig. 4. The framework functions as follows:

- The model is centralized and runs on the CPU, independent of the APs in the network.
- The model architecture, shown in Fig. 3, includes the signal selection block.
- The exchange scheme requires APs to relay signals to the CPU, with input comprising signals from all  $M$  APs in the network, as shown on the right side of Fig. 4.
- The model processes signals in parallel for each device, utilizing the selection block to leverage large-scale fading coefficients to identify the best cluster of AP signals for each device. Specifically, it selects the top  $T$  signals for device  $k$ , represented as  $[\mathbf{Y}_1, \mathbf{Y}_2, \dots, \mathbf{Y}_T]$ , as illustrated in Fig. 3.
- The model processes the signals through the hidden layers, producing  $T$  extracted feature vectors. These

are concatenated in the concatenation layer to detect the activity for all  $K$  devices, as each device has its own cluster of AP signals (though some clusters may overlap with different devices activities). It is essential to detect activity for all  $K$  devices within their respective clusters. For device  $k$ , the model selects their specific activity by ignoring the activities of the remaining  $K - 1$  devices, resulting in the predicted activity  $\tilde{a}_k$ , and ultimately producing the overall activity vector  $\tilde{\mathbf{a}}$ .

- Finally, the CPU applies a hard decision mechanism with a threshold  $\tau \geq 0$  to binarize the predicted values, yielding the final estimated activity vector  $\hat{\mathbf{a}}$ .

### F. TRAINING PHASE

In practical settings, our model operates initially in two distinct phases due to the absence of available training data. The initial phase, termed the transitional phase, entails the accumulation of the required data for model training. Subsequently, our research predominantly concentrates on the second phase, referred to as the permanent phase, during which the model uses an established dataset. The simulations and results of this study are rooted in the permanent phase, assuming that the model has progressed beyond the preliminary stage of data collection.

Let  $D_{tr} = \{(\mathbf{Y}_i, \mathbf{a}_i)\}_i$  where  $I = |D_{tr}| = 5 \times 10^4$  be a training dataset containing the received signal and the activity descriptor of a random access slot. Once the data are produced then we can train the model, the optimization problem can be stated as follows:

$$g(\mathbf{Y}, S, \vartheta) = \min_{\mathbf{X}} \|\mathbf{Y} - \mathbf{S}\mathbf{X}\|_F, \quad (19)$$

where  $\|\cdot\|_F$  is the frobenius norm, and the model parameters are indicated by  $\vartheta$ . A DNN is trained to map each input  $\mathbf{Y}_i$  to a desired estimated activity indicator  $\mathbf{a}_i$  via several successive layers of linear transformation interspersed with element-wise nonlinear transforms, given a collection of training examples  $D_{tr}$ . The input-output relationship for the hidden layers in a standard feed-forward neural network (FFNN) is expressed as follows:

$$\mathbf{x}^{(z)} = f(\mathbf{U}_z \mathbf{x}^{(z-1)} + \mathbf{b}_z), \quad (20)$$

where  $f(\cdot)$  denotes the non-linear activation function. In this equation,  $\mathbf{x}^{(z)}$  represents the output of the layer  $z$ , with  $\mathbf{x}^{(z-1)}$  being the input received from the previous layer  $z-1$ . The parameters of the network at this stage, namely the weight matrix  $\mathbf{U}_z$  between layer  $z-1$  and layer  $z$ , and the bias vector  $\mathbf{b}_z$  at layer  $z$ , are collectively represented by  $\vartheta$ . These parameters are learned and updated during training utilizing the adam optimizer. This optimizer, a popular variant of stochastic gradient descent, dynamically adjusts the learning rate for each parameter. The adam optimizer is particularly popular in ML due to its adaptability to handle sparse gradients and use of an adaptive learning rate mechanism, which allows it to converge in complicated

scenarios with resilience. We denote the output of the DL algorithm for the input sample  $(\mathbf{Y}_i, \mathbf{a}_i)$  as  $\tilde{\mathbf{a}}_i$ . For the network training, we use the binary cross-entropy loss [30] calculated over all the  $I = |D_{tr}|$  samples:

$$\mathbf{L}(D_{tr}) = - \sum_{i=1}^I [\mathbf{a}_i \log(\tilde{\mathbf{a}}_i) + (1 - \mathbf{a}_i) \log(1 - \tilde{\mathbf{a}}_i)]. \quad (21)$$

Using the back-propagation technique, we may propagate the loss all the way and train the parameters of the network. The loss function  $\mathbf{L}(D_{tr})$  is minimized during the training process by choosing the right parameters  $\vartheta$ . If after multiple epochs the loss function in (21) does not improve, the training ends. That is, the trained DL network estimates the activity descriptor with high accuracy.

There is an offline option for the training procedure. After the DNN parameters are learned, it is computationally less expensive to use this neural network for identifying active devices in new datasets (inference phase). The size of the new dataset for inference is typically 40% of the training data size, denoted as  $D_{tr}$  with size  $I = |D_{tr}|$ . During the inference phase, the neural network only requires a few vector-matrix multiplications, summations, and element-wise nonlinear operations.

#### IV. NUMERICAL RESULTS

This section explores the topic of improved connectivity in CF-mMIMO architectures, focusing on the evaluation and comparison of various activity detection algorithms in both cell-free and cellular mMIMO systems under near-realistic scenarios. The investigation begins with mathematically driven algorithms, including AMP, ISTA, and FISTA, as detailed in [25]. It then transitions to a data-driven approach leveraging neural networks, specifically the DNN architecture, employed thus far. To comprehensively evaluate the effectiveness of activity detection, we utilize the widely recognized receiver operating characteristics (ROC) curve, which represents the probability of detection ( $P_D = 1 - P_{MD}$ ) against the probability of false alarm ( $P_{FA}$ ). This method provides a robust framework for assessing detection performance across different operational thresholds.

##### A. SIMULATION MODEL

Our study covers a detailed scenario for both cell-free and cellular networks, defined by a diverse set of parameters. The key parameters for these scenarios are given in Table 3.<sup>1</sup>

<sup>1</sup>See Section II for a comprehensive analysis of simulation assumptions and parameters. Briefly, with  $\tau_c = 1$  ms and  $B_c = 200$  kHz yielding  $T_c = 200$  symbols and given  $K = 100$  devices, orthogonal pilot sequences might be deemed feasible. However, in our simulations, we employ non-orthogonal pilot sequences, even though  $K$  does not exceed  $T_c$  to improve the timing efficiency of our simulations. Given our objective to expand connectivity, this strategy allows for a potential increase in the number of devices. This approach is justified by its minimal effect on the outcomes.

TABLE 3. Simulation parameters.

Parameter	Cell-free	Cellular
<b>System</b>		
Area size ( $D^2$ )	1 Km <sup>2</sup>	
Edge distance	50 m	
Number of devices (K)	100	
Number of APs (M)	20	1
Number of antennas (N)	2	8
Pilot length (L)	40	
Minimum distance UE-AP	10 m	
AP Spacing	15 m	
Antenna height	12 m	
device height	1.5 m	
Carrier frequency (fc)	900 MHz	
Cluster size T	4	-
Sparsity level ( $\epsilon$ )	0.1	
<b>Coherence Block</b>		
Coherence Time $\tau_c$	1 ms	
Coherence bandwidth $B_c$	200 kHz	
Number of symbols $T_c$	200	
Reserved portion $\Delta$	20%	
<b>Channel Fading</b>		
Noise power $\sigma^2$	-109 dBm	
Small scale fading	Rayleigh	
Large scale fading	Path loss	3GPP standard
	Shadowing	$N(0, 1)$

##### B. DNN PARAMETERS TUNING: PERFORMANCE vs. COMPLEXITY

In this section, our primary focus is to evaluate the performance of DNN in the context of device activity detection in CF-mMIMO systems.

To achieve this goal and for simplicity, we conducted a thorough investigation into the architectural parameters of DNN, focusing initially on the decentralized approach. Our objective is to achieve a high level of accuracy in activity detection while mitigating the risk of over-fitting.

The tuning process involves careful consideration of the number of neurons within the hidden layers of the DNN architecture. We have conducted a thorough parameter search, varying the number of neurons  $V$  within the range  $\{128,$

160, 256, 320, 512, 640} and exploring different detector configurations with various numbers of intermediate hidden layers  $Z$  within the set {1, 2, 3, 4}. This meticulous parameter-tuning process is an essential step to optimize the DNN for accurate activity detection.

To objectively study the performance-complexity trade-off, the detectors are compared based on pareto efficiency. A detector  $(Z, V)$  is considered pareto-efficient if no alternative detector exists that reduces either the training losses, measured using binary cross-entropy on the training dataset in (21), or the complexity, assessed as the number of training parameters in (11), without adversely affecting the other metric. Since we are in the decentralized approach and, as previously stated, the concatenation layer has no effect, this scenario corresponds to the case where  $T = 1$  in the equation (11). The set of all pareto-efficient detectors, known as the pareto front, represents the available trade-off options. Switching from one pareto-efficient detector to another involves prioritizing either complexity or training loss. Conversely, a detector that is not pareto efficient should not be selected, as it is possible to improve at least one of the metrics without compromising the other.

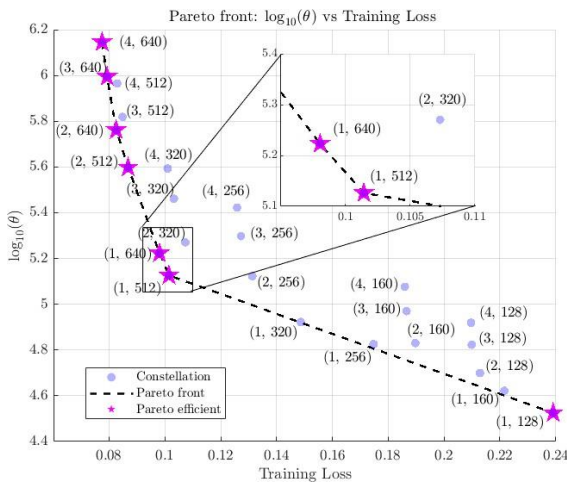


FIGURE 5. Pareto front : number of trainable parameters in the DNN vs training loss.

Analyzing the curve in Fig. 5, it is evident that increasing the number of parameters consistently decreases the minimum training loss. This trend is depicted in Fig. 5, where it is noticeable that increasing, the number of layers results in only a slight improvement in the validation loss for each value  $V$ . However, a substantial decrease in loss is observed when the number of neurons is increased for each  $Z$  value.

Fig. 5 illustrates that the optimal trade-off between complexity and loss is achieved with the detector configured as  $V = 512$  and  $Z = 1$ , as indicated by pareto-efficiency. Consequently, the DNN architecture is simplified to a single layer perceptron, which will be utilized for the remainder

of the simulations in both the centralized and decentralized approaches.

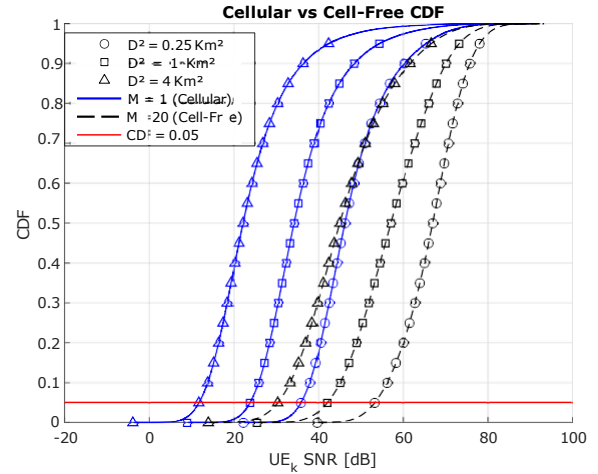


FIGURE 6. Active device SNR.

### C. SNR ANALYSIS RESULTS

Fig. 6 presents the cumulative distribution function (CDF) of the SNR for an active device in both a CF-mMIMO and a cellular network, based on the respective scenarios outlined in Table 3. The SNR is evaluated for devices transmitting at 200 mW in three coverage area sizes: 0.25 km<sup>2</sup>, 1 km<sup>2</sup> and 4 km<sup>2</sup> and in two configurations: 1 AP (cellular) and 20 AP (cell-free).

It is evident from Fig. 6 that the SNR achieved in the CF network, represented by dashed lines, significantly outperforms that of the cellular network, depicted by solid lines. This improvement indicates a lower likelihood of outage probability, translating to more reliable service for a larger number of devices. The enhanced SNR can be attributed to the carefully designed topology of access points and the realistic environmental model, which ensures devices are typically closer to an access point, benefiting from stronger channel gains and improved signal quality.

For simulation purposes, the SNR target at the dominant AP was set to ensure that 95% of the active devices meet the required SNR threshold to gain network access. This SNR target is depicted by the intersection of the plot lines with the reference line marked  $CDF = 0.05$ .

This analysis highlights the benefits of distributed AP deployment in the cell-free scenario, showcasing its ability to improve connectivity and minimize the risk of signal outages, which are essential for achieving robust and reliable performance. The use of markers distinguishes network configurations based on area size, underscoring the influence of this variable on SNR and overall network efficiency.

### D. ALGORITHM PERFORMANCE WITH VARIABLE SYSTEM PARAMETERS

In this section, we evaluate the performance of our proposed algorithms in both centralized and decentralized approaches

using various post-processing methods. The evaluation includes a comparison of all algorithms, including our models and those from the literature [14] [25], across different system parameters. Specifically, we analyze the pilot sequence length  $L$ , the total number of devices  $K$ , and the sparsity parameter  $\epsilon$ . All models are assessed under the scenarios outlined in Table 3. These parameters are critical for optimizing the system and provide valuable insights into the algorithms' adaptability and scalability in real-world deployments.

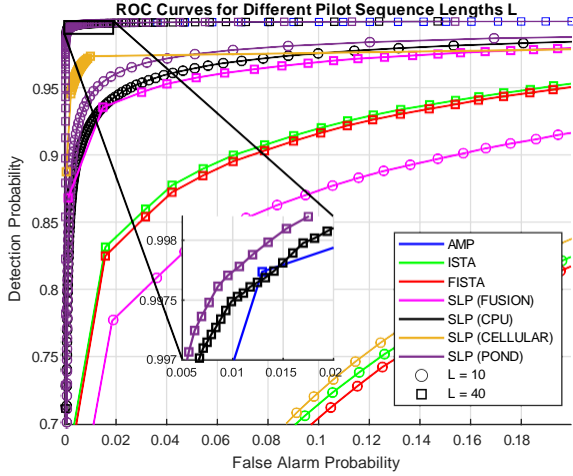


FIGURE 7. ROC curve analysis for different pilot sequence lengths  $L$ .

Fig. 7 presents the ROC curves for varying the pilot sequence lengths  $L$ , with all other parameters fixed as specified in Table 3. The results show a clear improvement in performance as the pilot length increases from 10 to 40. This enhancement is expected, as longer pilot sequences reduce the correlation between non-orthogonal pilots assigned to a fixed number of devices, improving device discrimination under the SLP algorithm. The plots also demonstrate that device activity detection performance is superior in cell-free massive MIMO networks compared to co-located MIMO networks, particularly as the pilot length increases. While the AMP algorithm struggles with shorter pilot lengths, it catches up as it  $L$  grows, though at a higher computational cost. Moreover, the SLP algorithm, in both the centralized CPU and distributed cases using weighting (POND), outperforms state-of-the-art algorithms across all values of  $L$ . However, longer pilot sequences occupy more of the coherence block, improving detection by lowering sequence correlation but reducing the symbols available for uplink and downlink data transmission. This trade-off may impact the overall data rate and increase the cost of transmission bandwidth.

Fig. 8 examines the performance of the models as the number of devices  $K$  increases, while keeping all other system parameters fixed. As shown, performance tends to degrade with higher device density. This behavior is expected, as increasing  $K$  enhances the correlation between

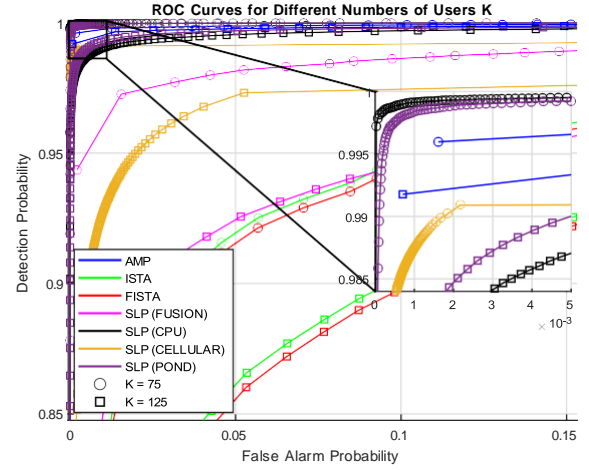


FIGURE 8. ROC curve analysis for different device numbers  $K$ .

pilot sequences due to more devices sharing a fixed resource pool, with the pilot sequence length held constant. In the model architecture (Fig. 3), the number of devices corresponds to the number of neurons in the last layer. A static input size combined with a high device count makes it more challenging for the network to differentiate between device signals, reducing discrimination performance. The results also highlight that CF networks outperform co-located networks across all scenarios. The AMP algorithm performs effectively for large values of  $K$ , while both the centralized and decentralized (POND) approaches surpass state-of-the-art algorithms when  $K \leq 100$ . A general comparison of different post-processing methods in the decentralized approach reveals that majority fusion decision yields lower performance compared to weighted methods. Assigning weights to access points based on priority (POND) or treating all APs equally, as in the fusion case (FUSION), significantly affects the performance.

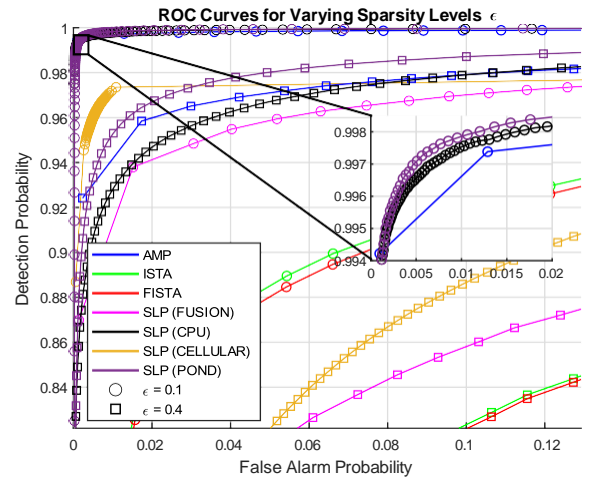


FIGURE 9. ROC curves for different sparsity parameters  $\epsilon$ .

Above all, this scenario illustrates the under-sampling ratio ( $\frac{L}{K}$ ), or the trade-off between the number of devices  $K$



and the length of the pilot sequence  $L$ . The performance of the algorithm can be optimized by establishing a balance between these variables, highlighting the significance of a comprehensive system design that takes into account the device density and available sequence lengths for a best system operation.

In Fig. 9, we analyze the performance of the models across varying sparsity levels  $\epsilon$ . As shown, performance decreases as  $\epsilon$  increases, which is expected due to higher activity levels leading to greater interference. The CF scenario consistently outperforms the cellular counterpart, demonstrating its superior capability in managing sparse activity detection. The SLP with ponderation post-processing function achieves the best performance across all sparsity levels, surpassing all other algorithms. At lower  $\epsilon$  values, both centralized and decentralized approaches are highly effective detectors. At higher  $\epsilon$  values, the centralized approach closely matches the performance of the AMP algorithm, establishing itself as a robust suboptimal detector.

Finally, the results emphasize the significance of employing both centralized and decentralized approaches with different post-processing methods. In the decentralized approach, the model learns features from a single received signal, whereas the centralized method processes a cluster of signals collected from the best APs. The decentralized approach with weighting demonstrates slightly better performance than the centralized CPU approach by leveraging external diversity through signal weighting, while the CPU approach explores diversity internally within the model. Both strategies have their strengths, and the optimal choice depends on balancing complexity and performance to identify the most suitable approach.

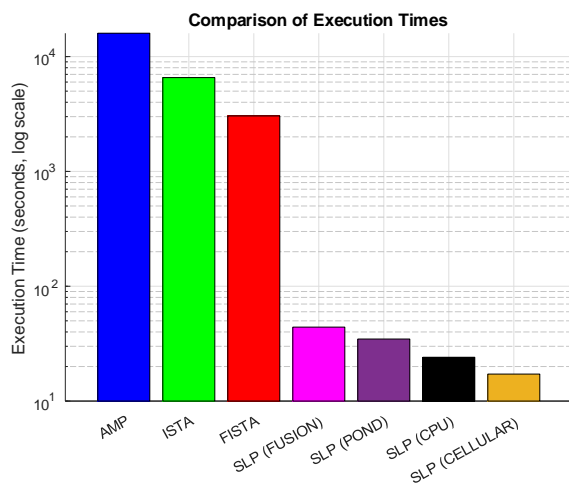


FIGURE 10. Comparison of execution times across all methods.

### E. TIME EFFICIENCY OF THE DL AND BASELINE ALGORITHMS

In CF-mMIMO systems, particularly in the context of mMTC applications, the sporadic and rapidly changing ac-

tivity of devices presents a unique challenge. In addition to performance, a key criterion for evaluating an activity detection system is its response time, especially when deployed in real-world environments. This study aims to address this challenge by examining the execution times of different algorithms, providing insights into their practical applicability.

Fig. 10 compares the inference execution times of all algorithms previously evaluated. For simplicity, each curve in figures 7, 8, and 9 is represented with the same color scheme in this figure. The simulations were conducted on a high-performance GPU computing setup designed to redirect jobs to GPU resources. The simulations utilized an NVIDIA HGX A100 GPU (graphics processing unit) cluster, configured with 9 nodes, each equipped with 4 GPUs and a total of 10,120,000 MB of memory per node. This setup ensured consistent and efficient computation for all algorithms.

For the iterative algorithms from the state-of-the-art [25], the number of iterations ( $t$ ) is a critical parameter influencing convergence. In our experiments, we followed the iteration numbers specified in [25], setting  $t = 18$  for AMP,  $t = 100$  for FISTA, and  $t = 235$  for ISTA. The comparison in Fig. 10, presented on a logarithmic scale, reveals the significant differences in execution times between data-driven and model-driven algorithms. Data-driven models demonstrate exceptionally low execution times compared to model-driven methods. However, as previously mentioned, the optimal choice depends on balancing complexity and performance.

For example, the distributed approach with the ponderation strategy offers a favorable trade-off, achieving fast response times with minimal performance degradation. On the other hand, the centralized (CPU) approach, while slightly less effective in terms of performance, provides even faster response times and serves as a strong suboptimal detector. Although model-driven methods can occasionally achieve higher performance, this comes at the cost of considerably longer execution times, as shown in Fig. 10.

This study serves as a preliminary analysis, focusing solely on execution times measured using the same hardware setup. Future work will extend this evaluation by calculating the number of multiply-accumulate (MAC) operations for all algorithms, enabling a more hardware-agnostic assessment of computational efficiency.

## V. CONCLUSION

This paper explored device activity detection in GF-RA scenarios within CF-mMIMO networks, introducing centralized and decentralized approaches built on a tailored deep learning framework. The findings highlighted the advantages of CF networks over cellular systems, including improved connectivity and reduced outage probabilities. Additionally, the analysis of execution times underscored the efficiency of data-driven algorithms compared to iterative, model-based methods. The proposed approaches demonstrated excellent performance in detecting active devices while ensuring low

computational complexity and fast inference execution times, making them well-suited for real-world mMTC deployments.

## REFERENCES

- [1] C. Bockelmann, N. Pratas, H. Nikopour, K. Au, T. Svensson, C. Stefanovic, P. Popovski, and A. Dekorsy, "mmtc in 5g: physical and mac-layer solutions," *IEEE Com. Magazine*, vol. 54, no. 9, pp. 59–65, 2016.
- [2] A.-S. Bana, E. de Carvalho, B. Soret, T. Abra $\tilde{c}$ o, J. C. Marinello, E. G. Larsson, and P. Popovski, "mMIMO for IoT connectivity," 2019.
- [3] T. L. Marzetta, "Noncooperative cellular wireless with unlimited numbers of base station antennas," *IEEE Tran. on Wireless Communications*, vol. 9, no. 11, pp. 3590–3600, 2010.
- [4] N. K. Pratas, H. Thomsen, C. Stefanovic, and P. Popovski, "Code-expanded random access for machine-type communications," in *2012 IEEE Globecom Workshops*, 2012, pp. 1681–1686.
- [5] J. H. Sørensen, E. de Carvalho, and P. Popovski, "mMIMO for crowd scenarios: A solution based on random access," in *IEEE GC Wkshps*, 2014, pp. 352–357.
- [6] E. Björnson, E. de Carvalho, E. G. Larsson, and P. Popovski, "Random access protocol for massive mimo: Strongest-user collision resolution (sucr)," in *IEEE ICC*, 2016, pp. 1–6.
- [7] J. Ding, D. Qu, and J. Choi, "Analysis of non-orthogonal sequences for grant-free ra with mMIMO," *IEEE Transactions on Communications*, vol. 68, no. 1, pp. 150–160, 2020.
- [8] M. B. Shahab, R. Abbas, M. Shirvanimoghaddam, and S. J. Johnson, "Grant-free non-orthogonal multiple access for iot: A survey," *IEEE Communications Surveys & Tutorials*, vol. 22, no. 3, pp. 1805–1838, 2020.
- [9] X. Chen, D. W. K. Ng, W. Yu, E. G. Larsson, N. Al-Dhahir, and R. Schober, "Massive access for 5g and beyond," *IEEE Journal on Selected Areas in Communications*, vol. 39, no. 3, pp. 615–637, 2021.
- [10] C. Bockelmann, H. F. Schepker, and A. Dekorsy, "Compressive sensing based multi-user detection for machine-to-machine communication," *Transactions on Emerging Telecommunications Technologies*, vol. 24, no. 4, pp. 389–400, 2013.
- [11] F. Monsees, M. Woltering, C. Bockelmann, and A. Dekorsy, "Compressive sensing multi-user detection for multicarrier systems in sporadic machine type communication," in *IEEE 81st VTC Spring*, 2015, pp. 1–5.
- [12] Z. Gao, L. Dai, Z. Wang, S. Chen, and L. Hanzo, "Compressive-sensing-based multiuser detector for the large-scale sm-mimo uplink," *IEEE Transactions on Vehicular Technology*, vol. 65, no. 10, pp. 8725–8730, 2016.
- [13] Y. Du, B. Dong, Z. Chen, X. Wang, Z. Liu, P. Gao, and S. Li, "Efficient multi-user detection for uplink grant-free noma: Prior-information aided adaptive compressive sensing perspective," *IEEE Journal on Selected Areas in Communications*, vol. 35, no. 12, pp. 2812–2828, 2017.
- [14] L. Liu and W. Yu, "Massive connectivity with massive mimo—part i: Device activity detection and channel estimation," *IEEE Transactions on Signal Processing*, vol. 66, no. 11, pp. 2933–2946, 2018.
- [15] K. Senel and E. G. Larsson, "Grant-free massive mtc-enabled massive mimo: A compressive sensing approach," *IEEE Transactions on Communications*, vol. 66, no. 12, pp. 6164–6175, 2018.
- [16] K. Senel and E. G. Larsson, "Device activity and embedded information bit detection using amp in massive mimo," in *2017 IEEE GC Wkshps*, 2017, pp. 1–6.
- [17] D. L. Donoho, A. Maleki, and A. Montanari, "Message-passing algorithms for compressed sensing," *Proceedings of the National Academy of Sciences*, vol. 106, no. 45, p. 18914–18919, Nov. 2009.
- [18] S. Haghghatshoar, P. Jung, and G. Caire, "Improved scaling law for activity detection in massive mimo systems," in *IEEE ISIT*, 2018, pp. 381–385.
- [19] Z. Chen, F. Sahrabi, Y.-F. Liu, and W. Yu, "Covariance based joint activity and data detection for massive random access with massive mimo," in *IEEE ICC*, 2019, pp. 1–6.
- [20] U. K. Ganesan, E. Björnson, and E. G. Larsson, "Clustering-based activity detection algorithms for grant-free random access in cell-free massive mimo," *IEEE Transactions on Communications*, vol. 69, no. 11, pp. 7520–7530, 2021.
- [21] U. K. Ganesan, E. Björnson, and E. G. Larsson, "An algorithm for grant-free random access in cell-free massive mimo," in *2020 IEEE 21st International Workshop on SPAWC*, 2020, pp. 1–5.
- [22] J. H. I. de Souza and T. Abra $\tilde{c}$ o, "Deep learning-based activity detection for grant-free random access," *IEEE Systems Journal*, vol. 17, no. 1, pp. 940–951, 2023.
- [23] Y. Bai, B. Ai, and W. Chen, "Deep learning based fast multiuser detection for massive machine-type communication," in *2019 IEEE 90th VTC2019-Fall*, 2019, pp. 1–5.
- [24] D. Donoho, "For most large underdetermined systems of equations, the minimal l-norm near-solution approximates the sparsest near-solution," *Communications on Pure and Applied Mathematics*, vol. 59, pp. 907–934, 07 2006.
- [25] Q. Zou and H. Yang, "A concise tutorial on approximate message passing," *ArXiv*, vol. abs/2201.07487, 2022. [Online]. Available: <https://api.semanticscholar.org/CorpusID:246035220>
- [26] 3rd Generation Partnership Project, "Study on channel model for frequencies from 0.5 to 100 ghz," 3GPP TR 38.901 V17.0.0 (2022-03), 3GPP, Valbonne, France, Technical Report TR 38.901, March 2022, release 17.
- [27] C. Wang, O. Y. Bursalioğlu, H. Papadopoulos, and G. Caire, "On-the-fly large-scale channel-gain estimation for massive antenna-array base stations," in *2018 IEEE International Conference on Communications (ICC)*, 2018, pp. 1–6.
- [28] A. Fengler, S. Haghghatshoar, P. Jung, and G. Caire, "Non-bayesian activity detection, large-scale fading coefficient estimation, and unsourced random access with a massive mimo receiver," *IEEE Transactions on Information Theory*, vol. 67, no. 5, pp. 2925–2951, 2021.
- [29] W. Tian, G. Rui, G. Liu, and D. Dong, "Efficient acquisition method for marine monitoring data based on compressed sensing," *IEEE Access*, vol. 7, pp. 159 797–159 807, 2019.
- [30] J. Nam, J. Kim, E. Loza Mencía, I. Gurevych, and J. Fuhrnkranz, *Large-Scale Multi-label Text Classification — Revisiting Neural Networks*. Springer Berlin Heidelberg, 2014, p. 437–452.